

Hydrogen concentration analyses using SIMS and FTIR: Comparison and calibration for nominally anhydrous minerals

Kenneth T. Koga, Erik H. Hauri, Marc M. Hirschmann, David Bell

▶ **To cite this version:**

Kenneth T. Koga, Erik H. Hauri, Marc M. Hirschmann, David Bell. Hydrogen concentration analyses using SIMS and FTIR: Comparison and calibration for nominally anhydrous minerals. Geochemistry, Geophysics, Geosystems, 2003, 4 (2), pp.1019. 10.1029/2002GC000378 . hal-01689355

HAL Id: hal-01689355
https://uca.hal.science/hal-01689355

Submitted on 28 Jan 2021

HAL is a multi-disciplinary open access archive for the deposit and dissemination of scientific research documents, whether they are published or not. The documents may come from teaching and research institutions in France or abroad, or from public or private research centers.

L'archive ouverte pluridisciplinaire **HAL**, est destinée au dépôt et à la diffusion de documents scientifiques de niveau recherche, publiés ou non, émanant des établissements d'enseignement et de recherche français ou étrangers, des laboratoires publics ou privés.

Geochemistry Geophysics Geosystems G3
AN ELECTRONIC JOURNAL OF THE EARTH SCIENCES
Published by AGU and the Geochemical Society

Article
Volume 4, Number 2
20 February 2003
1019, doi:10.1029/2002GC000378
ISSN: 1525-2027

Hydrogen concentration analyses using SIMS and FTIR: Comparison and calibration for nominally anhydrous minerals

Kenneth Koga
Department of Geology and Geophysics, University of Minnesota, Minneapolis, Minnesota 55455, USA

Currently at ENS-Lyon, CNRS UMR 5570, Laboratoire Sciences de la Terre, 46 Allee d'Italie, 69364 Lyon Cedex 7, France. (Kenneth.Koga@ens-lyon.fr)

Erik Hauri
Department of Terrestrial Magnetism, Carnegie Institution of Washington, 5241 Broad Branch Road NW, Washington, DC 20015, USA (hauri@dtm.ciw.edu)

Marc Hirschmann
Department of Geology and Geophysics, University of Minnesota, Minneapolis, Minnesota 55455, USA (hirsc022@tc.umn.edu)

David Bell
Department of Chemistry and Biochemistry, Arizona State University, Tempe, Arizona 85282, USA (David.R.Bell@asu.edu)

[1] We report analyses of hydrogen abundance in experimentally annealed and natural mantle minerals using FTIR and use these data to establish calibration lines for measurement of H_2O concentrations in olivine, pyroxenes, garnet, amphibole and mica by secondary ion mass spectrometry (SIMS). We have reduced the detection limit for H_2O analysis by SIMS to 2–4 ppm H_2O (by weight) through careful attention to sample preparation and vacuum quality. The accuracy of the SIMS calibrations depends on the choice of FTIR extinction coefficients; however, all of the calibrations reported here are shown to be consistent with measurements on standards whose H_2O abundance has been determined independently via manometry or nuclear reaction analysis. The resulting calibrations are accurate to 10–30% at the 95% confidence limit, with improvements possible through the use of higher-H_2O standards. Using our SIMS calibration, we determined hydrogen concentrations in coexisting olivine, orthopyroxene, and glass from a single melting experiment at 2 GPa and 1380°C. Olivine/melt and orthopyroxene/melt partition coefficients are equal to 0.0020 ± 0.0002 and 0.0245 ± 0.0015, respectively, and the orthopyroxene/olivine coefficient is 12 ± 4 (2σ uncertainties).

Components: 10,413 words, 7 figures, 6 tables.

Keywords: Water; hydrogen; mantle; mineral; ion probe; SIMS.

Index Terms: 1025 Geochemistry: Composition of the mantle; 1065 Geochemistry: Trace elements (3670); 1094 Geochemistry: Instruments and techniques; 3630 Mineralogy and Petrology: Experimental mineralogy and petrology.

Received 10 May 2002; **Revised** 24 October 2002; **Accepted** 31 October 2002; **Published** 20 February 2003.

Copyright 2003 by the American Geophysical Union

Koga, K., E. Hauri, M. Hirschmann, and D. Bell, Hydrogen concentration analyses using SIMS and FTIR: Comparison and calibration for nominally anhydrous minerals, *Geochem. Geophys. Geosyst.*, *4*(2), 1019, doi:10.1029/2002GC000378, 2003.

1. Introduction

[2] Most of the hydrogen in the Earth's mantle is likely dissolved as OH in nominally anhydrous minerals, in substitutions similar to those documented in minerals from mantle xenoliths [e.g., *Aines and Rossman*, 1984; *Smyth et al.*, 1991; *Bell and Rossman*, 1992a, 1992b; *Bell et al.*, 1995; *Snyder et al.*, 1995; *Kurosawa et al.*, 1997]. Considering the influence of hydrogen on mantle properties such as melting point [e.g., *Kushiro*, 1969; *Hirth and Kohlstedt*, 1996; *Karato and Jung*, 1998], rheology [e.g., *Chopra and Paterson*, 1984; *Karato et al.*, 1986; *Hirth and Kohlstedt*, 1996], conductivity [e.g., *Karato*, 1990] and seismic velocity [e.g., *Inoue et al.*, 1998], it is important to understand the distribution of H between mantle phases and the mass transfer processes that influence them. Yet, experimental determinations of the distribution of trace amounts of hydrogen remain limited [for example, see discussion of H partitioning in mantle, *Hirth and Kohlstedt*, 1996]. Available experimental data include pioneering studies of hydrogen solubility in olivine [*Bai and Kohlstedt*, 1992, 1993; *Bai et al.*, 1994; *Kohlstedt et al.*, 1996; *Matveev et al.*, 2001], garnet [*Ackermann et al.*, 1983; *Geiger et al.*, 1991; *Lu and Keppler*, 1997; *Withers et al.*, 1998], pyroxenes [*Skogby*, 1994; *Kohn*, 1996], and other high pressure minerals [e.g., *Meade et al.*, 1994; *Inoue et al.*, 1995; *Kohlstedt et al.*, 1996; *Bolfan-Casanova et al.*, 2000; *Murakami et al.*, 2002] and phase equilibria studies of hydrogen-bearing partially molten peridotite [*Kushiro*, 1972; *Green*, 1973; *Mysen and Boettcher*, 1975a, 1975b; *Hirose and Kawamoto*, 1995; *Kawamoto and Holloway*, 1997; *Gaetani and Grove*, 1998]. To date there exists only one experimental study of hydrogen partitioning between nominally anhydrous minerals and silicate melt [*Sweeney et al.*, 1997], and one study documenting hydrogen partitioning between natural boninite glass/orthopyroxene pairs [*Dobson et al.*, 1995].

[3] Among the difficulties contributing to limited understanding of hydrogen behavior in nominally anhydrous mantle minerals is the challenge of measuring accurately low abundances of hydrogen in small experimental samples. Some successes have been demonstrated using Fourier transform infrared spectroscopy (FTIR) on experimentally annealed, large (more than 1mm in length) olivine and garnet crystals [e.g., *Ackermann et al.*, 1983; *Geiger et al.*, 1991; *Kohlstedt et al.*, 1996; *Lu and Keppler*, 1997] or on experimentally annealed small crystals with unknown orientations [e.g., *Withers et al.*, 1998]. For optically anisotropic minerals, accurate FTIR analyses require identification of optical orienation [*Paterson*, 1982; *Libowitzky and Rossman*, 1997], which can be challenging in samples recovered from high-pressure experiments. FTIR has the capability to measure low hydrogen abundances as well as provide information on hydrogen speciation, but element-partitioning experiments involving a melt phase normally do not produce crystals amenable to oriented FTIR analysis. Nuclear reaction analysis (NRA) applied to measurements of hydrogen abundance [e.g., *Bell et al.*, 2002] can attain detection limits of 2–4 ppm H_2O and does not require crystal orientation, however the spatial resolution of this technique is limited to hundreds of microns. Elastic recoil detection analysis (ERDA) can attain spatial resolution below 100 μm and is also insensitive to crystal orientation [*Sweeney et al.*, 1997], but the results of this technique currently give elevated H_2O abundances for olivine that are not in agreement with solubility considerations and FTIR measurements [*Bell et al.*, 2002].

[4] Considering designs of potential experiments to investigate hydrogen equilibration between multiple condensed phases, an analytical procedure for hydrogen analysis that combines low detection

limit, high spatial resolution and insensitivity to crystal orientation would be of considerable utility. The ion microprobe offers these advantages, and in this paper we demonstrate that advances in secondary ion mass spectrometry (SIMS) hold new promise for quantitative analysis of hydrogen in nominally anhydrous phases.

[5] The main obstacle for achieving accurate measurements of hydrogen in low-concentration phases by SIMS is the high level of background hydrogen endemic to typical analytical conditions, as hydrogen is a relatively abundant contaminant in mass spectrometer vacuums, in primary ion sources, and adsorbed onto sample surfaces [*Yurimoto et al.*, 1989; *Ihinger et al.*, 1994; *Deloule et al.*, 1995]. All previous SIMS studies of water abundance in silicates have encountered either high background or coarse spatial resolution, and are not applicable for analysis of nominally anhydrous minerals with H_2O contents less than 100 ppm. *Hinthorne and Andersen* [1975] reported a detection limit of 120 ppm H_2O by weight (all ppm H_2O references in this paper are in weight units) with a calibration from various hydrous minerals. *Sisson and Layne* [1993] reported glass water content down to 1.0 ± 0.1 wt% using a Cameca IMS3f ion probe at the Woods Hole Oceanographic Institution. Detailed silicate glass analyses by *Deloule et al.* [1995] revealed a background level of 1600 ppm H_2O using Cameca IMS3f at CRPG-CNRS (Nancy, France) with 2–6 nA O^- primary beam with −80 V energy offset. The same group later reduced the background to 300 ppm H_2O by using a 10–15nA O^- primary beam with −100V offset [*Sobolev and Chaussidon*, 1996]. Substantial improvements in SIMS techniques were demonstrated by *Yurimoto et al.* [1989] and *Kurosawa et al.* [1992], who achieved a low-blank calibration of a Cameca IMS3f at University of Tsukuba with olivine, quartz and glasses, using a 100–150nA O^- primary beam and −100V secondary acceleration voltage offset (energy filtering). The probe diameter of these studies was 100 μm, but the spatial resolution was improved to 60 μm with use of a field aperture. Importantly, the detection limits for these studies (6–7 ppm H_2O) were determined from the analysis of a known anhydrous material (quartz with 0.75 ppm H_2O). Recently, *Hauri et al.* [2002] used a Cameca IMS6f at the Department of Terrestrial Magnetism of the Carnegie Institution at Washington (DTM) with a Cs^+ primary beam and no energy offset and achieved a detection limit of 20–30 ppm H_2O and a spatial resolution of 5–10 μm.

[6] The goal of this contribution is to detail improved analyses of small quantities of hydrogen at high spatial resolution in a variety of nominally anhydrous minerals. To this end, we describe improved procedures for achieving a low detection limit for hydrogen by SIMS and document this by analyzing crystals with known very low H_2O contents. We also combine and compare FTIR and SIMS analyses of experimentally annealed olivine and orthopyroxene, along with new SIMS analyses of olivine, pyroxenes and garnets analyzed previously by FTIR, manometry and nuclear reaction analysis [*Bell and Rossman*, 1992a, 1992b; *Bell et al.*, 1995, 2002]. Data are also given for various amphiboles and micas [*Deloule et al.*, 1991]. We use these analyses to construct separate SIMS calibration curves for each of these phases. Finally, we report some preliminary determinations of hydrogen partition coefficients between olivine, opx, and hydrous silicate melt and we compare advantages of FTIR and SIMS for measurements of hydrogen concentration in experimental charges requiring high sensitivity.

2. Standards

[7] The standards used in this study come from several sources (Table 1). Olivine and orthopyroxene with a range of H_2O concentrations were made by annealing at elevated pressure (0.3 and 2 GPa) and temperature (1000°–1200°C). One high-concentration olivine standard, DLK-16, annealed at 13 GPa and 1100°C, is from the study of *Kohlstedt et al.* [1996]. Selected olivine, orthopyroxene, garnet, clinopyroxene, amphibole and mica natural minerals are from previously published work [*Bell and Rossman*, 1992a, 1992b; *Bell et al.*, 1995; *Bell et al.*, 2002; *Deloule et al.*, 1991] and basalt standards are those described by *Hauri et al.* [2002]. The synthetic forsterite is from *Morioka* [1980]. Finally, minerals with very low hydrogen (>40–200 ppb H_2O), experimentally dehydrated

Table 1. Compositions of Nominally Anhydrous and Hydrous Mineral Standards

	Fo90 Olivine[a]	SynFo68 Olivine	GRR1012 Olivine	KLV-23 Olivine	KBH-1 opx	India opx[b]	Kenya opx	MON-9 garnet	ROM263-9 garnet	ROM263-25 garnet	ROM263-52 garnet
SiO_2	40.88	37.37	40.82	40.32	54.68	54.52	57.24	42.2	41.5	41.68	41.87
TiO_2	–	–	0.03	0.03	0.11	–	–	1.25	1.17	1.14	0.98
Al_2O_3	–	–	0.01	0.05	4.73	1.91	–	20.39	21.18	21.15	20.52
FeO	9.86	28.56	8.76	12.27	5.88	13.43	8.63	10.89	10.85	9.9	8.95
MgO	49.26	34.07	50.51	47.47	32.92	30.15	34.12	19.52	19.21	19.83	20.52
CaO	–	–	0.03	0.08	0.86	–		4.62	4.54	4.6	4.42
Na_2O	–	–	0.02	0.03	0.12	–	–	0.11	0.1	0.1	0.09
K_2O	–	–	–	–	–	–	–	0	–	–	–
H_2O	–	<0.0001	0.022	0.012	0.0186	–	<0.0001	0.0056	0.004	0.0032	0.0015
Totals	100	100	100.2	100.26	99.32	100.01	100	98.99	98.55	98.4	97.35

	PMR-53 cpx	Hydrous Minerals	Bamble Amphibole	Bita Hochee Amphibole	Illimaussaq Amphibole	Alpes Amphibole	Seljas Amphibole	Kipawa Amphibole	CO1a Phlogopite	Mica Fe Biotite	M114 Biotite
SiO_2	54.78		51.48	41.36	49.57	54.25	57.12	46.42	37.98	33.83	38.03
TiO_2	0.35		0.34	4.38	0.62	0.1	0	0.82	0.53	2.44	1.85
Al_2O_3	2.83		4.08	12.43	0.71	4.2	0.06	8.58	16.3	18.58	19.45
FeO	6.87		8.45	11.31	32.42	7.53	7.86	13.14	9.07	23.61	16.98
MgO	18.3		18.2	12.77	0.01	18.69	20.18	14.43	16.68	5.03	12.84
CaO	13.26		11.94	10.72	0.34	11.57	12.35	11.23	0	0.01	0
Na_2O	2.13		1.59	2.51	7.25	0.7	0.11	2.55	0.33	0.23	0.11
K_2O	0.05		0.27	1.93	3.24	0.06	0	1.08	9.22	9.05	8.57
H_2O	0.0286		2.03	1.37	1.6	2.81	2.47	1.52	2.71	2.78	3
Totals	98.6		98.38	98.78	95.76	99.92	100.15	99.78	92.82	95.56	100.83

[a] Representative major element composition for experimentally hydrated olivines DLK-16, a270, a2880, a278, a286 and a287, and olivine megacryst KLV-23.
[b] Representative major element composition for experimentally hydrated orthopyroxenes a270, a2880, a281, a286 and a288.

Table 2. Water Contents and SIMS Data for Standards

Sample name	$^1H/^{30}Si$ (2σ)	H_2O wt% (2σ)	Mthd, Ref.	Sample name	$^1H/^{30}Si$ (2σ)	H_2O wt% (2σ)	Mthd, Ref.
Basalt				***Orthopyroxene***		**(×10⁴)**	
run 24	8.78(22)	5.54(5)	M,1	KBH-1	0.026(3)	186(20)	M,6
run 17	6.9(2.0)	5.33(5)	M,1	a270	0.035(6)	134(47)	F,12
run 30	8.47(16)	4.81(5)	M,1			*268(94)*[b]	
ALV1833-1	3.36(18)	2.43(30)	F,2	a280	0.026(2)	122(43)	F,12
ALV1833-11	2.13(24)	1.20(50)	F,2			*244(86)*[b]	
30-2	1.20(1)	0.60(6)	F,3	a281	0.029(6)	108(38)	F,12
Bouvet CHN	1.06(2)	0.52(5)	M,4			*216(76)*[b]	
SLNT	1.01(3)	0.49(5)	M,4	Enstatite India	0.019(3)	60(21)	F,12
ALV 526-1	0.357(5)	0.25(3)	M,4			*120(42)*[b]	
1OC-1	0.305(4)	0.24(3)	M,4	a286	0.012(2)	36(13)	F,12
ALV519-4-1	0.390(22)	0.17(2)	F,5			*72(26)*[b]	
40-2	0.276(3)	0.15(2)	F,3	a288	0.009(2)	22(8)	F,12
KI-79-6	0.202(7)	0.11(2)	F,8			*44(16)*[b]	
				Enstatite Kenya+	0.00066(6)	*0.2(1)*[b]	F,12
Garnet		(×10⁴)					
MON-9	0.0032(12)	56(11)	M,6	***Clinopyroxene***		(×10⁴)	
ROM263-25	0.0019(8)	32(6)	F,11				
ROM263-52	0.0079(70)	15(3)	F,11	PMR-53	0.038(5)	286(30)	M,6
MON-9HT+	0.00034(2)	0.10(5)	F,6	PMR-53HT+	0.00065(3)	0.10(5)	F,6
Olivine		(×10⁴)		***Amphibole***			
DLK16	0.410(52)	1090(382)	F,7	Bamble	3.59(40)	2.03(20)	M,10
		3820(1340)[a]		Bita Hochee	2.52(14)	1.37(14)	M,10
KLV-23	0.0112(31)	120(20)	NR,9	Kipawa	2.77(5)	1.52(15)	M,10
GRR1012	0.0264(47)	220(40)	NR,9	Illimaussaq	5.33(42)	1.60(16)	M,10
a270	0.0104(1)	30(10)	F,12	Seljas	3.04(80)	2.47(25)	M,10
		105(35)[a]		Alpes			
a280	0.0260(40)	50(17)	F,12	(*C-parallel*)	3.76(12)	2.81(30)	M,10
		175(60)[a]		(*C-perp.*)	3.46(20)	2.81(30)	
a278	0.0123(1)	21(7)	F,12				
		74(25)[a]		***Mica***			
a286	0.0069(8)	17(6)	F,12	CO1a phlog.			
		60(21)[a]		(*C-parallel*)	5.23(30)	2.71(30)	M,10
a287	0.0042(8)	17(6)	F,12	(*C-perp.*)	5.24(26)	2.71(30)	
		60(21)[a]		M114 biotite			
SynFo68+	0.00046(3)	*0.04(2)*[a]	F,12	(*C-parallel*)	6.33(6)	3.00(30)	M,10
				(*C-perp.*)	6.20(40)	3.00(30)	
SynFo100+	0.00045(2)	*0.04(2)*[a]	F,12	Mica-Fe			
				(*C-parallel*)	5.33(8)	2.78	M,10
				(*C-perp.*)	5.47(36)	2.78	

[a] Olivine concentrations in italics calculated from the method of *Bell et al.* [2002].
[b] Opx concentrations in italics increased by factor of two for consistency with manometry (see text). Methods(Mthd.): F, FTIR; M, manometry; NR, nuclear reaction. The plus denotes the minerals used as "zero standard." References are as follows: (1) *Mandeville*, personal communication; (2) *Stolper and Newman* [1994]; (3) A. Sobolev, personal communication; (4) *Stolper* [1982]; (5) *Fine and Stolper* [1994]; (6) *Bell et al.* [1995]; (7) *Kohlstedt et al.* [1996]; (8) *Hauri et al.* [2002]; (9) *Bell et al.* [2002]; (10) *Deloule et al.* [1991]; (11) *Bell and Rossman* [1992b]; (12) this study.

and verified by FTIR, were used to determine the level of hydrogen background during SIMS analysis. SIMS data along with H_2O abundances of these standards are given in Table 2.

3. Experimental Procedures

[8] Large optically clear crystals of olivine and orthopyroxene were used as the starting material for hydrogen bearing annealing experiments. Olivine, $(Mg_{1.8}Fe_{0.2})SiO_4$, is from San Carlos, Arizona, and orthopyroxene, $(Mg_{1.58}Fe_{0.39}Al_{0.03})(Si_{1.96}Al_{0.03})O_6$, is from Kangan, Andhra-Pradesh, India. These crystals were first oriented to their optical axes as estimated from their crystal habits, and then more precisely by x-ray microdiffraction at the University of Minnesota. Oriented crystals were cut to rectangular prisms with three different

edge lengths, which permitted tracking of the orientation of crystals during preparation. The final crystal dimensions were approximately 1.2 × 0.8 × 0.5 mm. Water contents of starting olivine and orthopyroxene crystals were <2 ppm and 60 ppm H_2O, respectively, as determined by FTIR. The starting minerals were not preconditioned at fixed oxygen fugacity prior to annealing.

[9] Oriented crystals were loaded in a gold or nickel capsule (4–5 mm in length, 2–3 mm inner diameter). First a 1 mm thick layer of powdered talc was loaded in the capsule, and 1–2 microliters of double-distilled H_2O was added with a microsyringe. In some cases, liquid D_2O (>98% D) was added to create variable H_2O concentrations in the experimental charges. This technique allowed us to synthesize crystals with a wide range of H_2O concentrations within a limited pressure range. If the fluid droplet was not absorbed by the talc powder, additional talc was added and packed flat. The olivine and opx crystals were placed in the capsule carefully, so that their optical orientation could be recovered after the experiment. The capsule was then welded shut.

[10] Annealing experiments were performed in a 1/2 inch bore piston cylinder apparatus at University of Minnesota. Further details of the experimental design, temperature, and pressure calibrations are given in *Xirouchakis et al.* [2001]. The oxidation state of the charge was not controlled, but *Xirouchakis et al.* [2001] showed that this assembly fixes f_{O2} within the stability field of wustite. Conditions of individual experiments, expected f_{O2} and capsule material are further described in Table 3.

[11] Initially, we attempted to recover single crystals from quenched charges by carefully peeling the Au capsule with a razor blade, but crystals fractured during depressurization and quenching, making it impossible to recover large single crystals. Instead, we analyzed oriented crystals by sectioning the experimental charge perpendicular to the long direction. Available data on diffusion of hydrogen in olivine and pyroxene [*Mackwell and Kohlstedt*, 1990; *Ingrin et al.*, 1995] allow estimation of the time required to approach equilibrium partitioning of hydrogen. Diffusion is slower in pyroxene, and assuming $D^{opx} = 2 \times 10^{-11}$ m^2/s at 1150°C, a 1 mm slab of opx will equilibrate in 4 hours. The extent of homogeneity was checked by searching for variation in hydrogen abundance in the ion probe spot analyses.

4. Analytical Procedures

4.1. Infrared Spectroscopy

[12] FITR measurements employed a Nicolet Series II Magna-IR System 750 FTIR equipped with Nic-Plan IR microscope and KBr beam splitter at the Material Characterization facility at University of Minnesota. Apertures were normally set to 100 μm diameter illumination, smaller apertures were used when it was necessary to reduce the area of IR transmission. The IR signals were collected for wave number resolution of 2 cm^{-1} and from 128 to 1024 scans depending on aperture size and absorption intensity. This method is described in detail by *Kohlstedt et al.* [1996].

[13] Recovered experimental crystals were doubly polished for FTIR analysis. Typically, crystals were ground to a thickness of approximately 100–200 μm using alumina power or diamond lapping films, with final polishing done with one micron grit. During polishing, the crystal was fixed to a metal disk using acetone-soluble superglue. The glue was then dissolved in acetone for 20 min, then in ethanol and distilled water for 5 min each.

[14] After polishing, samples were placed in a vacuum oven at 110°C and 2 kPa for at least 2 hours, and preferably more than 12 hours. Omission of vacuum oven treatment resulted in appearance of IR absorption peaks near 2700–2800 cm^{-1}, which are characteristic of C-H bonding and therefore of acetone or ethanol contamination (Figure 1). For such samples, broad absorption peaks attributable to molecular H_2O were also present between 3100 and 3700 cm^{-1}. With more rigorous drying, C-H and molecular H_2O peaks diminished, and narrow peaks between 3300 and 3400 cm^{-1} and between 3500 and 3600 cm^{-1} became more prominent. These sharper peaks were inferred to represent stretching vibrations in lattice-

Table 3. Conditions and Capsule Materials of H and D Bearing Synthesis Experiments[a]

Sample	Capsule	rel. fO_2	Fluid	oliv	opx	T (°C)	P(GPa)	Hours
a270	Au tube weld seal, MgO	wu	H-talc	x	x	1100	1.8	2.0
a278	Pt tube weld seal, MgO	wu	H-talc	x		1150	2.3	2.2
a280	Au long tube weld, MgO	wu	D-fl/H-talc	x	x	1150	2.3	3.0
a281	Au tube weld seal, MgO	wu	H-talc		x	1000	2.5	24.0
a286	NiO cup, Au gasket, P seal, MgO	Ni metal	D-fl/H-talc	x	x	1150	2.3	4.2
a287	Au tube weld seal, graphite	wu	D-fl/H-talc	x	x	1150	2.3	5.0
a288	Ni cup, Au gasket, P seal, MgO	Ni metal	D-fl/H-talc	x	x	1150	2.3	4.6
Melting experiment								
b13	Ni cup Au gasket P seal, MgO	Ni metal	D-fl/H-talc			1380	1.8	44.8

[a] Ni cups were sealed by pressure using Au gasket. Relative f_{O2} are estimated by *Xirouchakis et al.* [1999]. NiO capsule was recovered as Ni metal, thus f_{O2} is more reduced than NiO. Subsequently, Ni metal capsules were used. Methods of fluid introduction: H-talc, natural talc powder; D-fl, >98% D_2O fluid, which was introduced to vary the composition of fluid.

bound OH^- ions. It is interesting to note that standard drying ovens or short duration in a vacuum oven were insufficient to eliminate surface-adsorbed molecular H_2O. This problem may be even more significant for studies employing powders, and we emphasize that spurious analytical results may result from measurements of H in experimentally annealed samples if stringent drying procedures are not implemented.

[15] The concentration of H_2O in minerals was quantified by the strength of absorption in the 3750–3000 cm^{-1} region (Figure 1) using Beer's law, which describes the linear relationship between number of infrared active bonds in a matrix and the quantity of absorption. The Beer's law extinction coefficient determines the correspondence between absorption and concentration. We used two methods to calculate H_2O concentrations from FTIR spectra in olivine and orthopyroxene. The first method uses the empirical extinction coefficients and integration methods described by *Paterson* [1982]. We chose to use this method in order to maintain consistency with measurements of experimental samples previously analyzed at Minnesota [*Kohlstedt et al.*, 1996]. The second method is modified from the technique described by *Bell et al.* [2002] applied to the same spectra. These two quantification methods gave similar H_2O concentrations for natural orthopyroxene, as observed previously [*Bell et al.*, 1995]. However, mutual agreement among SIMS, FTIR and manometry requires that the H_2O abundances for the experimentally annealed orthopyroxenes in our study are approximately twice as high as measured by FTIR using the technique of *Paterson* [1982]. This difference may result from a combination of factors, including detailed differences in crystal orientation, light polarization and integrated absorbance between different FTIR techniques, and different IR-sensitive substitution mechanisms between natural and experimentally hydrated orthopyroxenes. For olivine, the method of *Bell et al.* [2002] gives H_2O abundances 3.5 times higher than the method of *Paterson* [1982] for the olivines in our study. Both sets of olivine and orthopyroxene concentrations are reported in Table 2, together with H_2O abundances of all other standards used in this study.

[16] Uncertainties in hydrogen concentrations determined by FTIR stem from a number of potential sources, including (1) different crystal orientations and sources of IR light (polarized versus non-polarized), (2) reproducibility of absorption peaks, (3) correction of IR absorption baseline at low signal-to-noise ratios, (4) measurement of sample thicknesses, and (5) imperfections in crystal orientation. We found the reproducibility of absorption peaks to be <2 cm^{-1} for wave number and for <1% relative for intensity on the basis of repeated analyses of the sample spot. Assignation of an accurate baseline correction is more problematic. The OH absorption peak appears on top of a broad slope (Figure 2) and there is no rigorous theory to determine the proper method of subtracting this background. Different polynomial baseline corrections on a same absorption curve result in 15–20% variation of H_2O determination. Sample thickness contributes

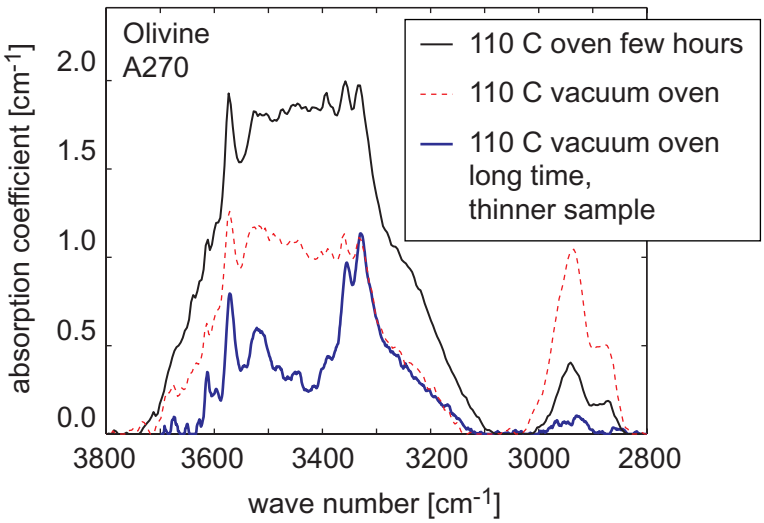


Figure 1. FTIR absorption peaks in an experimentally annealed olivine sample. This shows that the reduction of broad OH^- absorption peak occurs when more stringent drying procedure is applied, and as a result absorption spectra show sharp OH absorption peaks that characterize OH incorporation in olivine crystalline structure. The reduction of broad OH peak also correlates with the reduction C-H absorption peak around 2950 and 2850 cm^{-1}.

much less to measurement uncertainty, as thickness is measured with a precision of approximately 2 μm, which is just 1 to 2% relative of the total sample thickness. Finally, the uncertainty in orienting the crystal is estimated to be less than 2° and this adds an uncertainty of less than 2% in H_2O concentration. Thus the chief uncertainty in the precision of OH^- by FTIR stems from background connections and is approximately 20%.

[17] The minimum quantity of OH absorption detectable above the baseline corresponds to approximately 2 ppm H_2O for a 100 μm-thick wafer. Theoretically, a thicker sample allows measurement

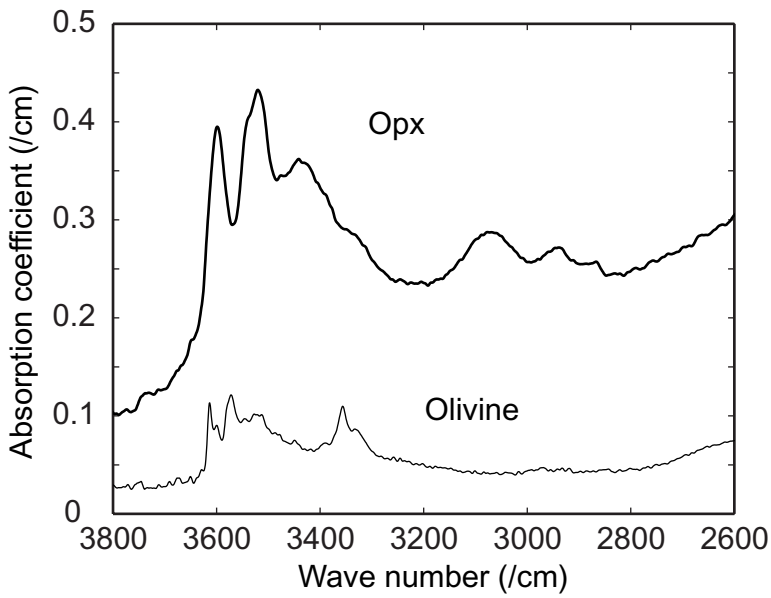


Figure 2. FTIR absorption peaks of orthopyroxene(opx) and olivine. Baselines are sloped with increase in absorption toward low wave number. Intensity of absorption is normalized by sample thickness (absorption coefficients).

of lower concentrations, but experimental samples thicker than 100 μm generally have fractures that preclude a clear optical path. The "zero" standards listed in Table 1 do not have similar flaws, as they were all prepared from gem-quality single crystals. Their H_2O contents range from 40–200 ppb H_2O based on FTIR spectra of >1 mm-thick wafers.

4.2. SIMS Analysis

[18] Initial reconnaissance studies for the working curve calibrations were done on Cameca IMS3f instrument at Woods Hole Oceanographic Institution using a primary beam of O^- ions and measuring positive secondary ions, following *Deloule et al.* [1995]. These initial studies suffered from high hydrogen backgrounds similar to those described previously, owing to a combination of inadequate analysis vacuum, low yield of H^+ ions due to a high energy offset, and contributions from hydrogen located on sample surfaces and primary beam source. These hydrogen backgrounds were, in most cases, higher than the actual hydrogen content of most nominally anhydrous minerals.

[19] Subsequent ion probe measurements on experimental charges were performed on a Cameca IMS6f at DTM. This method uses a Cs^+ primary ion beam and measurement of negatively charged secondary ions, and has been described previously [*Hauri et al.*, 2002]. For quantitative calibration of the ion probe, the minerals and glasses listed in Table 1 were measured, and calibration curves were constructed by determining functions relating water content (as determined by FTIR, manometry or nuclear reaction analysis) and $^1H/^{30}Si$ ratio determined by the ion probe.

[20] Analytical conditions of the DTM IMS6f ion microprobe were identical to those described in *Hauri et al.* [2002]. Instrumental vacuum conditions were improved by baking the entire instrument for at least 24 hours before an analytical session. Analytical vacuum was improved further by leaving the electron gun on for 12 hours at an electron current of 2.5 μA, resulting in desorption and pumping of hydrogen from the interior surfaces of the instrument. The electron beam current was then reduced to 0.3–0.4 μA for the analyses [*Hauri et al.*, 2002]; in this way, hydrogen desorption from the instrument by the electron beam does not contribute to the hydrogen background. Alignment of the electron gun was periodically checked by attaining uniform secondary ion intensity within the sputter crater by observing the H ion image on a hydrous glass (ALV1833-1 or ALV1833-11). The energy window was narrowed during this procedure to improve the energy resolution of the charge-compensated ion image.

[21] This study improves on the hydrogen backgrounds reported by *Hauri et al.* [2002] mainly through improvements in sample preparation and analytical vacuum. The use of standards with extremely low but known H_2O contents is critical to accurate determination of the hydrogen detection limit, so that the measured detection limit is not limited by the hydrogen abundance of the lowest standard. The ultimate vacuum of the DTM ion probe analysis chamber, without samples inserted or beams on, is 2×10^{-10} torr; this vacuum increases to 5×10^{-10} torr with ion and electron beams on. As a result, samples and standards must be prepared so that they do not degrade the vacuum further. This is achieved by attaching the samples to aluminum disks with a small amount of superglue, or pressing the samples into holes filled with indium metal. Epoxy is to be avoided at all costs, as numerous measurements of the hydrogen detection limit suggest that epoxy forms a hydrogen-bearing gaseous boundary layer at the surface of a degassing sample, which contributes to the hydrogen background although it may not degrade the overall vacuum pressure.

[22] The SIMS analyses were performed using the following procedure. A primary beam 20 μm in diameter was rastered over a 50 μm × 50 μm area for 1–3 min prior to analysis. During this time, we monitored secondary ion images of ^1H, ^{12}C and ^{35}Cl projected on the channel plate. This procedure helped avoid inclusions and cracks, which appear as bright features on the projected image. After each beam spot was carefully examined, the raster was stopped and a field aperture inserted to permit transmission of ions only from the central 8 μm of the 20 μm beam crater, thus avoiding transmission

of hydrogen ions from the edge of the sputter crater and the surface of the sample. Counting times for ^{1}H, ^{2}D, and ^{30}Si, were 5, 10, and 1 s respectively. Sometimes $^{12}C/^{30}Si$ and $^{35}Cl/^{30}Si$ ratios were measured as a monitor of possible surface contamination, and analyses showing spuriously high values of these ratios discarded.

[23] SIMS calibrations are regressions of ion probe signals compared to known concentrations. The former is normally taken as the intensity ratio of two elements, one being the element of interest and the other a matrix element common to many phases. In this study, standard H_2O concentrations are plotted against measured $^{1}H/^{30}Si$ ratios. This provides a robust analysis which is little influenced by primary beam fluctuations or by ionization efficiency changes owing to matrix effects [*Shimizu and Hart*, 1982].

4.3. Crystallographic Orientation

[24] Ion probe analyses were made in one amphibole and three micas to investigate the possibility that the SIMS H_2O calibrations could depend on crystallographic orientation. Analyses were made parallel and perpendicular to the C-axis of these minerals, and the results are given in Table 2. Comparison of data obtained with C-parallel and C-perpendicular crystal orientations show clearly that there is no dependence of the measured $^{1}H/^{30}Si$ ratios on crystallographic direction. The SIMS techniques are thus generally applicable to minerals of any orientation.

5. SIMS Detection Limit For H_2O in Silicates

[25] Detection limits of hydrogen in SIMS analyses are usually estimated from Y-intercepts of linear regressions of data from standards [e.g., *Ihinger et al.*, 1994]. However, this method may be inaccurate if uncertainties on regressed data are large or if H concentrations in standards are substantially greater than the detection limit. Accurate estimates of detection limits require standards with H_2O abundances known to be substantially lower than the expected background. Consequently, we measured olivine, orthopyroxene, clinopyroxene and garnet "zero" standards (Table 1) with H_2O abundances demonstrably less than 1 ppm. These "zero" standards gave consistent measured H_2O abundances of 2–4 ppm by weight by SIMS. Standard data used in the calibration regressions were corrected for this background.

[26] In an effort to reduce further the hydrogen detection limit, we explored the use of energy filtering [*Shimizu and Hart*, 1982]. The change of $^{1}H/^{30}Si$ for the "zero" olivine standard SynFo68 over various secondary acceleration voltage offsets is shown in Figure 3 in black diamonds; in this experiment, energy filtering was achieved by moving the energy slit at constant sample voltage. These data show a decrease of $^{1}H/^{30}Si$ with increase of the offset of the secondary acceleration voltage and seemed initially to suggest that 50V of energy filtering might reduce the hydrogen background. However, parallel measurements of ALV 1833-1 glass demonstrated that the reduction in $^{1}H/^{30}Si$ is actually the result of changing ion yields with energy offset (resulting in an increasingly larger calibration slope), rather than a change in the actual hydrogen background. Open symbols in Figure 3 show the intensity of ^{1}H and ^{30}Si against the offset of the secondary acceleration voltage for the same measurements. Intensity of ^{1}H and ^{30}Si signal decreases approximately two orders of magnitude over 50V offset. In the end, energy filtering resulted in a decrease in sensitivity without an actual reduction of hydrogen background and thus we elected not to use it.

6. Results and Discussion

6.1. Choices of IR Extinction Coefficients

[27] *Paterson* [1982] developed an empirical calibration of integrated extinction coefficients for O-H bonds in silica glass, quartz, and other glasses and water. Based on the assumption that O-H bonds are oriented in a single direction, the method employs a geometric coefficient which allows the approximate determination of OH^- concentration from FTIR measurement of a single crystal with known orientation. Although uncertainties in this calibration were thought by Paterson to be about 30%, it has been widely adopted

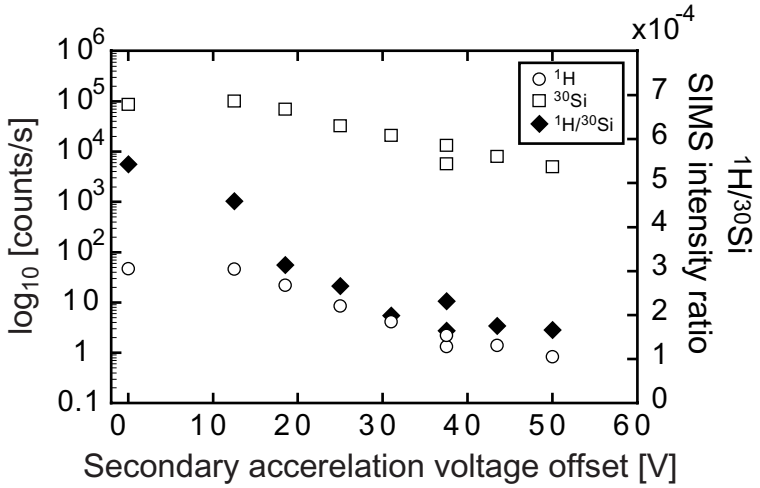


Figure 3. Reduction of secondary ion intensity of ^{1}H and ^{30}Si with increase of secondary acceleration voltage offset for analyses of the "zero" olivine standard SynFo68. The intensity of ^{1}H and ^{30}Si is read from the vertical axis on left. Increase of the offset reduces the intensity by a factor of 20. $^{1}H/^{30}Si$ intensity ratio is read from vertical axis on right side. While intensity dropped over factor of 20, $^{1}H/^{30}Si$ ratio dropped only factor of four reflecting a change in relative sensitivity factors of H and Si. Energy filtering was not effective in lowering the H_2O detection limit.

[e.g., *Bai and Kohlstedt*, 1992, 1993; *Kohlstedt et al.*, 1996; *Lu and Keppler*, 1997; *Mei and Kohlstedt*, 2000a, 2000b] because in certain favorable circumstances the geometric coefficient potentially obviates the need for more difficult polarized light observations in multiple crystallographic directions. However, recent studies [e.g., *Libowitzky and Rossman*, 1997; *Bell et al.*, 2002] have shown that it can result in non-systematic underestimates of hydrogen concentrations, and this is suggested in our SIMS data for olivine and orthopyroxene. Here we discuss the systematic uncertainties that may be introduced by the choice of extinction coefficients.

[28] Even if the application of a geometric coefficient may limit accuracy, it still may provide good reproducibility and internal consistency for similar spectra. For example, *Bai and Kohlstedt* [1992, 1993] assumed that the OH bond is oriented parallel to the **c** direction of olivine and documented systematic changes of H concentration as a function of pressure, temperature, and oxygen fugacity. However, *Miller et al.* [1987] demonstrated that OH^- absorption in natural olivine is strongly pleochroic, which prevents absorption measurements from only one orientation from accounting for all the OH^- present [*Libowitzky and Rossman*, 1996; *Libowitzky and Beran*, 1995]. Unless the crystallographic sites of dissolved hydrogen significantly change significantly with experimental conditions, the methods used by *Bai and Kohlstedt* [1992, 1993] likely underestimate the concentration of OH^- in olivine.

[29] Recently, *Bell et al.* [2002] have shown that Paterson's method accounts for only 25–45% of OH concentrations in olivine. We have tested the *Paterson* [1982] and *Bell et al.* [2002] extinction coefficients and calculation methods by comparing H_2O abundances in olivine calculated for the same IR spectra using a geometric correction factor of 1/2 for both methods; the Bell method results in olivine concentrations higher by a factor of 3.5 compared to the former (Figure 4). Table 2 lists H_2O concentrations for our olivine standards using both methods. While *Bell et al.* [2002] used IR data obtained from three orthogonal direction, we have come to the similar conclusion using a geometric correction factor. This suggests that IR data reduction using geometric collection can determine the abundance of water to first order.

[30] In the present study, in addition to minerals analyzed by FTIR, we utilized two samples of olivine (GRR1012, KLV-23) with H_2O abundance

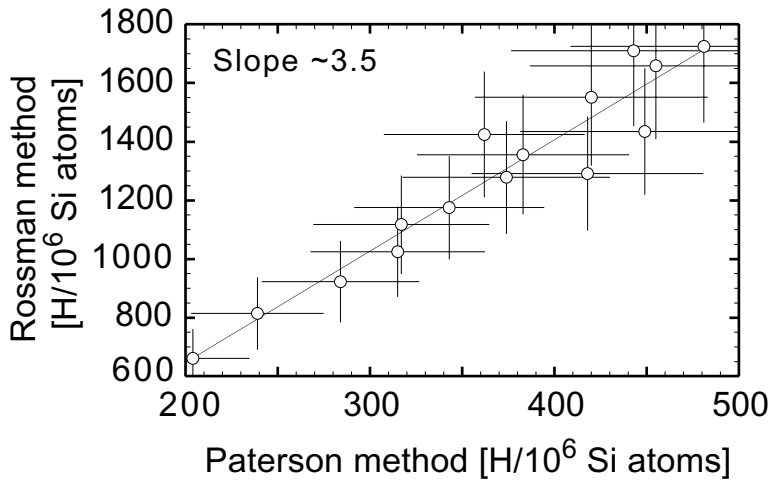


Figure 4. Comparison of H_2O concentrations in olivine determined by applying two different calculation methods to the same set of FTIR spectra. The method of *Paterson* [1982] applies variable extinction coefficients to the range of 3650 to 3000 cm^{-1}. The method of *Bell et al.* [2002] uses a single extinction coefficient applied to integrated absorption coefficient for the same range. The same geometric correction of 1/2 is applied. Water contents by the method of *Bell et al.* [2002] are 3.5 times higher on average than those calculated from the method of *Paterson* [1982]. The higher olivine concentrations were preferred for determining the SIMS calibration for olivine (see text).

determined by nuclear reaction analysis [*Bell et al.*, 2002], and one sample each of orthopyroxene, clinopyroxene and garnet in which hydrogen concentrations were determined by manometry [*Bell et al.*, 1995] (Table 2). Thus, all of the SIMS calibrations reported here rely in part on standards whose H_2O abundances have been determined by two different methods. Furthermore, we will show that the consistency of the SIMS calibration curves suggests that our choice of extinction coefficients is accurate to within the uncertainty in the calibration fits (±12–30%).

6.2. Calibration Lines and Error Assessments for SIMS

[31] Results of blank-corrected SIMS calibrations are shown for basalt, olivine, pyroxenes, garnet and hydrous phases in Figure 5 and regression coefficients are given in Table 3. We present three different calibration fits, linear, forced-zero linear, and log linear, in order to test for consistency and possible skewing by high-concentration standards. Ion probe data are fitted to FTIR, manometry and nuclear reaction H_2O data using York's regression method for uncorrelated errors [*York*, 1969].

[32] When examining the SIMS calibrations for nominally anhydrous minerals, we considered the consistency of the calibration lines and placed a premium on reproducing samples for which OH measurements from nuclear reaction analysis (GRR1012, KLV-23 olivines) and manometry (KBH-1 opx, PMR-53 cpx, MON-9 garnet, hydrous phases) are available. This results in SIMS calibrations that are less likely to inherit systematic errors from a particular corroborating method.

6.3. Basalt Calibration

[33] Hydrogen concentrations of basalt standards are higher than minerals, and are thus better constrained (Figure 5a). Some basalt glasses (run24, 17, and 30) showed large spatial variations in $^1H/^{30}Si$ which we presume reflect sample heterogeneity. It is included in the regression, but its large uncertainty means it has little impact on the weighted fit. In practice, calibration trends are quadratic for glasses with concentrations >1.5 wt% H_2O, but a linear calibration is adequate for samples with <1.5 wt% H_2O [*Hauri et al.*, 2002]. Prior to each ion probe session, we checked the basalt glass calibration for consistency with previous sessions. The trend shown in Figure 4a is consistent that of *Hauri et al.* [2002]

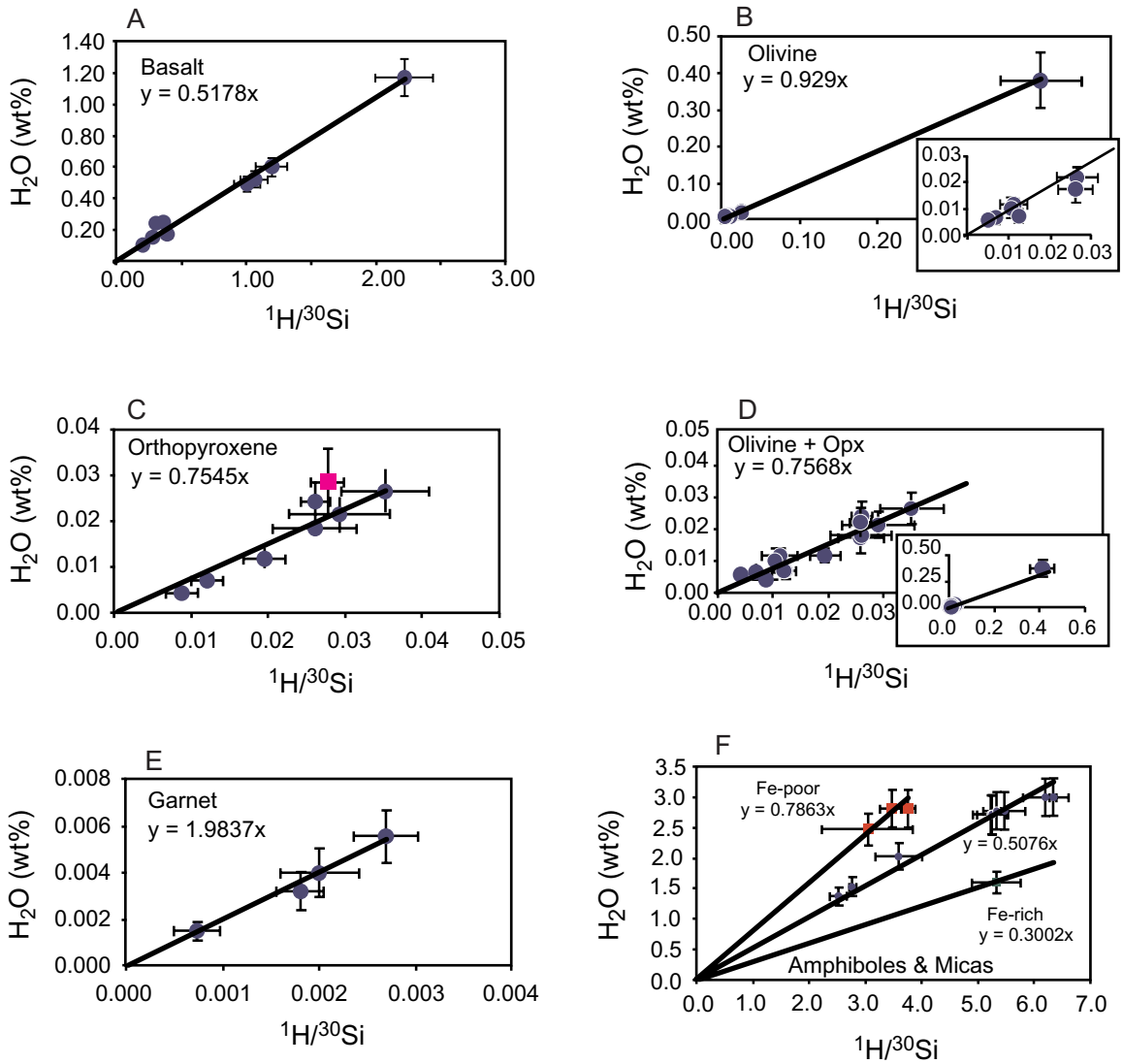


Figure 5. SIMS calibration lines for (a) basalt, (b) olivine (including DLK-16), (c) orthopyroxene, (d) olivine and orthopyroxene combined, (e) garnet and (f) hydrous phases. Calibrations are determined by linear regression of measurements by ion probe ($^1H/^{30}Si$) against standard H_2O concentration (Table 2). Black line corresponds to regression model #2 (forced zero). For olivine, H_2O concentrations used are those calculated from IR spectra using the method of *Bell et al.* [2002]; the resulting calibration line passes very close to olivine KLV-23 (120 ppm by nuclear reaction analysis). The combined olivine-orthopyroxene calibration excludes olivine DLK-16, but passes within error of its H_2O content.

and the uncertainty on the coefficient is 10% [*Hauri et al.*, 2002].

6.4. Olivine Calibration

[34] Olivine calibration is shown in a linear scaled plot (Figure 5b). Replicated points are shown when the measurement variation exceeded the error range determined by the counting statistics. SIMS analyses show that this variation is caused by heterogeneous distribution of H in some olivines. There exists a good correlation of $^1H/^{30}Si$ ratios with H_2O concentrations among the experimentally annealed olivines analyzed by FTIR. The slope of the calibration line appears to be dominated by the high hydrogen concentration sample (DLK-16), yet the distribution of low-H_2O standards about the calibration line is normal. Regres-

sion without DLK-16 gives a calibration slope 20% lower. Regression employing the H_2O contents calculated from the method of *Paterson* [1982] yield a trend that underestimates the H_2O abundance of GRR1012 and KLV-23 olivines by more than a factor of two. However, using the H_2O contents calculated from the method of *Bell et al.* [2002] the calibration trend passes very close to these olivines, and has a zero intercept within error (Figure 5b). The uncertainty on the slope of this calibration is 20%.

6.5. Pyroxene Calibration

[35] The single Ca-bearing clinopyroxene analyzed (PMR-53) suggest a SIMS calibration line intermediate between those for basalt and olivine; analysis of more clinopyroxene standards is a priority for future improvements. The correlation between $^1H/^{30}Si$ ratios and H_2O content for the experimental Ca-poor orthopyroxenes is good, but the resulting correlation underestimates the data for KBH-1 opx (H_2O determined by manometry) by a factor of two. Again, this difference is the result of systematic differences in FTIR methods and data reduction between the methods of *Paterson* [1982] and *Bell et al.* [2002].

[36] Using the higher H_2O abundances for orthopyroxene given in Table 2, an excellent calibration line is obtained (Figure 5c). This particular calibration is supported by the consistency of the calibration with the manometry data for KBH-1 opx, and it gives a slope that is similar to the calibration for olivine (Table 4). This latter observation is expected given the chemical similarity and mean atomic weight of olivine and orthopyroxene. Since the concentration range of the opx standards is only a factor of five, addition of an orthopyroxene with higher concentration could improve the precision of the calibration.

[37] Table 4 shows that the slopes of the SIMS calibration lines for olivine and orthopyroxene are very similar, as would be expected from their chemical similarity. Thus a consistent SIMS calibration is obtained by regressing the data for olivine and orthopyroxene together (Figure 5d). Table 4 includes two combined olivine-orthopyroxene regressions, with and without the high-H_2O olivine DLK-16. The difference in slope is 20%, similar to the regression uncertainties for either mineral. The regression without DLK-16 gives a more even distribution of standards about the calibration line.

Table 4. Regression Parameters for SIMS Calibrations

	A(slope)	±2σ	B	±2σ	MSWD
Basalt					
$y = Ax + B$[a]	0.51	0.06	0.016	0.055	3.8
$y = Ax$[b]	0.52				
$y = Ax^{Bc}$	0.53	0.10	0.94	0.19	8.2
Olivine					
$y = Ax + B$	0.93	0.20	0.0010	0.0038	3.8
$y = Ax$	0.93				
$y = Ax^B$	0.81	0.60	0.97	0.21	5.7
Opx					
$y = Ax + B$	0.91	0.16	−0.0039	0.0027	1.2
$y = Ax$	0.75				
$y = Ax^B$	0.71	0.40	1.20	0.19	0.4
Olivine and Opx[d] (with DLK-16)					
$y = Ax + B$	0.94	0.17	−0.0029	0.0021	5.8
$y = Ax$	0.93				
$y = Ax^B$	0.65	0.52	0.96	0.28	6.3
Olivine and Opx[d] (w/o DLK-16)					
$y = Ax + B$	0.77	0.17	0.00003	0.0034	5.7
$y = Ax$	0.76				
$y = Ax^B$	0.65	0.52	0.96	0.28	6.3
Garnet					
$y = Ax + B$	1.97	0.60	−0.00001	0.0009	0.4
$y = Ax$	1.98				
$y = Ax^B$	2.09	0.84	1.01	0.30	0.2
Cpx					
$y = Ax + B$	1.04	0.27	−0.00019	0.0002	0.0
$y = Ax$	1.04				
$y = Ax^B$	1.23	3.00	0.94	0.28	0.2

[a] Used *York* [1969] uncorrelated error weighted regression.
[b] The regression was forced to go through zero.
[c] Log linear fit using *York* [1969]; when B = 1, identical to (1) with zero intercept Olivine and orthopyroxene curves use higher H2O values from Table 2.
[d] Olivine and orthopyroxene regressed together (including and excluding DLK-16).

6.6. Garnet Calibration

[38] Four garnet standards were used to calibrate the garnet calibration curve (Figure 5e). The hydrogen abundance of the highest-concentration garnet (MON-9) was determined by manometry, while the remaining garnets were measured by FTIR using an extinction coefficient derived from IR measurements on MON-9 [*Bell et al.*, 1995]. The regression shows the positive correlation of $^1H/^{30}Si$ but

the error on the slope is the largest of all the calibrations (30%). The slope of the SIMS garnet calibration is quite different from those of the other minerals, and it should be pointed out that the manometry measurements on MON-9 garnet were particularly difficult and used large amounts of sample (up to 3 grams) from which it is can be difficult to exclude contaminant H_2O entirely [*Bell et al.*, 1995]. For example, a reduction of all of the garnet concentrations (Table 2) by a factor of two would bring the slope of the garnet calibration more in line with those for the pyroxenes and olivine. Future NRA analyses of garnet will contribute to reducing such uncertainties in the accuracy of the SIMS garnet calibration.

6.7. Calibrations for Hydrous Minerals

[39] Six amphiboles and three micas [*Deloule et al.*, 1991] were analyzed to produce calibrations for hydrous minerals (Table 2); the data are shown in Figure 5f. Most of the amphiboles and all of the micas give a calibration line that is very similar in slope to the basalt calibration (Figure 5a). The exceptions are the Fe-rich Illimaussaq gedrite, which gives a shallower slope (0.30) and the Fe-poor and Mg-rich Seljas and Alpes amphiboles which give steeper slopes (around 0.80) similar to those for olivine and orthopyroxene. The dependence of the hydrous mineral calibrations on Fe content is shown in Figure 6. The nominally anhydrous minerals are generally consistent with this relationship with the exception of the garnet calibration, which shows the steepest slope of all the minerals.

6.8. Consistency of Calibrations

[40] Linear fitting of a trend over a large range of concentration can result in over-weighting high-value data points and high-concentration standards may dominate regression slopes, as for olivine (Figure 5b). To explore this possibility, we compared linear regressions and log linear regressions, which reduce the leverage of high concentration data points (Table 4). The forms of the equations are:

$$Y = aX + b \tag{1}$$

for linear regression where Y and X are values of observation and regression, a and b are slope and Y-intercept. The log linear regression is given by

$$\log(Y) = b' \log(X) + a' \tag{2}$$

and the power law form of the above equation is,

$$Y = 10^{a'} X^{b'}. \tag{3}$$

When exponential factor b' is one and intercept b is zero, the linear and log linear equations are identical and the slope a is equal to $10^{a'}$. The departure of b' from unity indicates an exponential curvature to the regression when plotted in linear space. For regressions with widely spaced points, in which the Y-intercept of both is close to zero, the similarity of slopes provides an indication of whether the linear regression is dominated by high-value data points. However, for closely spaced data points, such as for the garnet and orthopyroxene data (Figures 5c and 5e), the errors on the slope from the log linear regression are very large when this regression is projected in linear space.

[41] All of the SIMS data have been regressed with linear (with both unconstrained and forced-zero intercepts) and log linear functions, and the results are given in Table 4. In all cases, the slopes of linear and log linear fits are identical within errors while the exponential factor is equal to one within the errors. Thus, the calibration curve regression is indeed linear and high concentration data are not overly skewing the fit, with the exception of olivine DLK-16. In theory, blank-corrected calibration trends should go through the origin. The fact that the York's regressions do so provides independent confirmation that background correction is accurate. We choose to use the slopes of the forced zero intercept regressions as the calibration coefficients hereafter, including the combined regression (without DLK-16) for olivine and orthopyroxene.

7. Olivine-Orthopyroxene-Melt Partition Coefficients

[42] Hydrogen partition coefficients among olivine, orthopyroxene and silicate melt were deter-

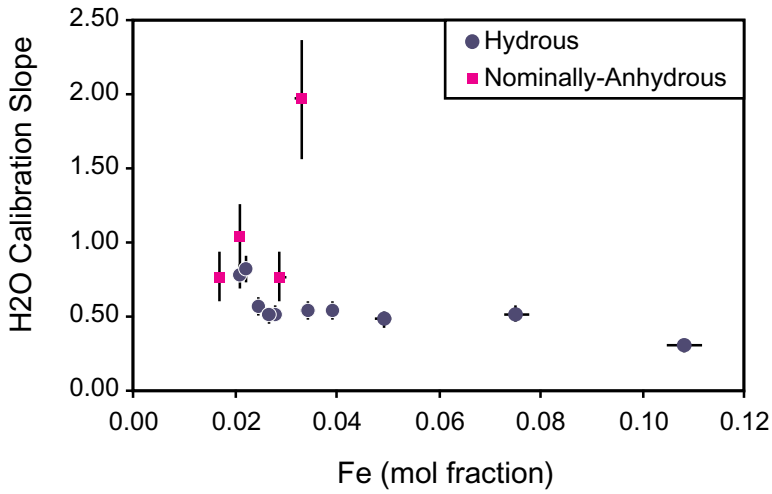


Figure 6. Changes in H_2O calibration slope with Fe content of minerals. Hydrous and nominally anhydrous minerals (except garnet) follow the same trend.

mined in a melting experiment at 1380°C and 2 GPa for 45 hours. A bulk composition (54.9% SiO_2, 0.1% TiO_2, 4.9% Al_2O_3, 2.4% FeO, 7.5% CaO, 22.1% MgO, 0.2% NaO, 1.6% H_2O, ~6% D_2O) was annealed in a Ni pressure-sealed capsule. Hydrogen and deuterium were introduced in the form of natural talc and deuterium oxide fluid by syringe. After the anneal, the sample crystallized olivine and opx from melt (Table 5). The quenched sample was then polished and analyzed by SIMS.

[43] The quenched experiment consisted of olivine and opx crystals embedded in glass (Figure 7). Partition coefficients for olivine-opx-melt pairs were determined from $^1H/^{30}Si$ ratios for all phases, with water abundances calculated from to the SIMS calibration line (Table 6). Because a SIMS calibration for deuterium has not been determined, only the ratios of $^2D/^{30}Si$ were used to calculate deuterium partition coefficients. There is good agreement between determined partition coefficients without matrix correction between H and D. This agreement suggests that the validity of H distribution data confirmed by low-background analyses of D. Although the precision of deuterium distribution data is better than that of hydrogen, the accurate values of deuterium partition coefficients should be calculated following determination of the respective deuterium calibration coefficients for SIMS.

[44] The olivine/melt partition coefficients reported in Table 6 are more than a factor of ten lower than those reported by *Sweeney et al.* [1997], and this is due to the relatively high H_2O contents reported for olivine from that study. Our partition coefficients are in general agreement with those of D. R. Bell, G. R. Rossman, and R. O. Moore (Abundance and partitioning of OH in a high-pressure magmatic system: Megacrysts from the Monastery kimber-

Table 5. Composition of Coexisting Phases at 1.8 GPa, 1380°C From Experiment B13[a]

wt. %	opx	olivine	melt
SiO_2	49.5(5)	35.0(4)	47.0(8)
Al_2O_3	7.3(8)	0.14(2)	16.9(6)
FeO	3.5(2)	4.2(1)	4.5(1)
MgO	22.7(4)	25.7(10)	7.9(10)
CaO	1.3(1)	0.12(2)	12.1(5)
NiO	16.4(5)	36.6(13)	4.4(8)
Na_2O			0.95(5)
H_2O	0.024(2)	0.002(1)	0.97(5)
D_2O	0.095	0.008	3.87(9)
Total	100.6(4)	102.0(5)	98.5(12)

[a] Analysis by WDS using a JEOL 8900 microprobe, except for H_2O and D_2O concentration. H_2O is determined by SIMS using methods described in this paper. D_2O is estimated from H_2O using the constraint that four times more D_2O was introduced to the starting composition. However, comparing $D/^{30}Si$ to $H/^{30}Si$, deuterium intensities are only about 1.3–1.6 times higher than hydrogen. The accurate D_2O concentration can not be determined owing to a lack of deuterium concentration standards, but the estimated values here are probably the highest possible values. Uncertainties are reported as 1 sigma.

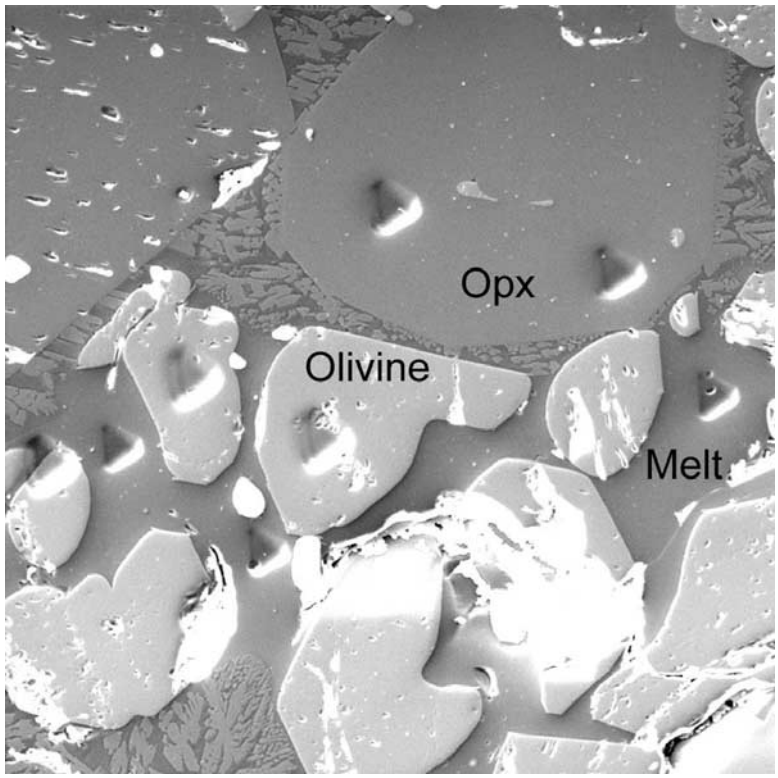


Figure 7. SEM image showing experimentally synthesized phases and craters made by ion probe and size of ion probe pits are ~20 μm. Partition coefficients are calculated as shown from the ion probe analyses (Table 5).

lite, South Africa, manuscript submitted to *Journal of Petrology,* 2002) inferred from H_2O distributions in kimberlite megacrysts from Monastery, South Africa and an estimated H_2O abundance for the host kimberlite. Our olivine/melt partition coefficients are at the low end, and our opx/melt partition coefficients are at the high end of these megacryst data. Consequently, our opx/olivine partition coefficient is higher than that observed by Bell et al. (submitted manuscript, 2002). Although our data are too preliminary to warrant detailed interpretation, they demonstrate the potential of SIMS for experimental partitioning studies of hydrogen and other volatile elements in high-pressure experiments. Our experiment also provides broad constraints regarding partitioning at mantle pressures. For a mantle mineral assemblage of 50% olivine, 35% orthopyroxene, 13% clinopyroxene and 2% spinel, the bulk solid/melt partition coefficient for H suggested by our data is approximately 0.009, on the basis that twice as much H_2O partitions into clinopyroxene compared to orthopyroxene [*Bell and Rossman*, 1992a, 1992b]. This value is essentially identical to that of Ce [*Salters et al.*, 2002], suggesting a similarity of partitioning of hydrogen and Ce that has been inferred from many studies of H_2O in basalt glasses [e.g., *Michael*, 1988, 1995; *Dixon et al.*, 1997]. We also note that the measured opx/olivine partition coefficient is in general agreement with the factor of 5 assumed by *Hirth and Kohlstedt* [1996].

[45] We hasten to note that these partition coefficients have several important limitations. First, the melt and mineral compositions are Ni-rich

Table 6. Partition Coefficients ($D^{A/B}$) at 1.8 GPa, 1380°C From Experiment B13, Measured by Ion Probe (±2σ)

	Hydrogen[a]	Deuterium[b]	H_2O[c]
D(opx/melt)	0.017(2)	0.017(2)	0.0245(15)
D(olv/melt)	0.0016(2)	0.0012(2)	0.0020(2)
D(opx/oliv)	11(2)	14(2)	12(4)

[a] Intensity ratios of hydrogen used.
[b] Intensity ratios of deuterium used.
[c] Concentration ratios calculated from calibration curves.

owing to capsule contamination and this may affect partitioning relative to that expected in natural compositions (Table 5). Because the concentration of network modifiers in the melt is comparable to that in basalt, we consider it unlikely that the effect of Ni on hydrogen partition coefficients are large. Second, our single experiment does not allow evaluation of Henry's law for these phases. Distribution of H between minerals and melt may have distinct dependencies on H_2O fugacity [e.g., *Hirth and Kohlstedt*, 1996] or other intensive variables. Further, different minerals may have greatly different activity/composition relations for H. Thus, FTIR studies indicate more than one possible substitution site for H in olivine [*Miller et al.*, 1987; *Libowitzky and Beran*, 1995] and opx shows broader OH absorption peaks than olivine (Figure 2) suggesting larger variations of OH bond strength. Either observation could suggest possible non-Henrian behavior for hydrogen activity in mineral phases. If the concentration-activity relationship for hydrogen is non-Henrian, a partition coefficient cannot be used for describing behavior of hydrogen in mantle minerals and melts.

8. Comparisons and Conclusions

[46] This study allows comparison of SIMS and FTIR analyses of low concentrations of hydrogen in minerals. In many ways, SIMS and FTIR are complimentary techniques. The ion microprobe allows in situ analyses of small single spots, but FTIR provides information on substitution mechanisms. The chief differences between the two are spatial resolution, sensitivity and sample preparation procedures.

[47] Lateral and depth resolution is better for SIMS than for FTIR. During a typical 10 minute analysis, the depth of the ion probe sputter crater is only a few microns, while FTIR integrates absorption over the full thickness of the sample wafer. For typical analytical conditions in this study, the ion probe primary beam diameter was approximately 20 μm and the analytical resolution improved to 5–10 μm diameter with the use of a field aperture. Although analysis areas as small as 20 μm are attainable by micro-FTIR, the practicality of analysis requires larger spot sizes (generally 50 × 50 μm) because 100μm thick nominally anhydrous samples do not contain sufficient water in sample volumes smaller than this.

[48] Using the lateral resolutions and the detection limits of SIMS and FTIR, it is possible to directly compare the minimum number of atoms required for each analytical method. The actual volume of material analysed in SIMS is approximately 20 μm^3 and its detection limit is approximately 4 ppm; the minimum number of H atoms required for analysis is $\sim 1 \times 10^7$. FTIR requires $\sim 3 \times 10^{10}$ H atoms, assuming the detection limit to be approximately 1 ppm for 100 μm thick sample. The FTIR detection limit is based on our FTIR measurements on various samples. On an equal-atom basis, SIMS is thus more than three orders of magnitude more sensitive than FTIR for abundance measurements of hydrogen.

[49] It is also possible to compare the sensitivity of SIMS and FTIR by directly comparing the conditions of detection limits. During ion probe analysis, "zero" standards gave hydrogen counts of tens of ions per second, two orders of magnitude above the typical background noise of the counting system (<5 counts per minute), thereby resulting in the previously described blank of 2–4 ppm. The source of this residual hydrogen background is unknown, but may correspond to ions entering the mass spectrometer at oblique angles through the field aperture. In contrast, the H_2O detection limit for FTIR can be substantially lower than 1 ppm with the used of thick samples, but it is limited mainly by the optical quality of thick wafers and the accuracy of baseline subtraction at low signal-to-noise ratios.

[50] Finally we emphasise that accurate FTIR analysis of anisotropic phases places demanding geometrical requirements on preparation of experimental samples, and that these may not be practical for small volume experimental charges. The relatively simple analytical geometry and high spatial resolution of SIMS yields considerable advantages in such studies.

Acknowledgments

[51] Dave Kohlstedt and Jeff Allwardt are thanked for providing their experimental products as standards. Many thanks to Jackie Dixon, Sally Newman, Penny King, Charlie Mandeville, Etienne Deloule and George Rossman for providing standards, and to Jianhua Wang for convincing the 6f to realize its potential in spite of itself. KTK gives thanks for helpful discussions from Shun Karato, Mark Zimmerman, Tetsu Kogiso and Maik Pertermann for experimentation, and Nobu Shimizu, Graham Layne, and Estelle Rose for providing WHOI SIMS and advice at the initial stage of this project. MMH gratefully acknowledges NSF support through OCE9876255. The DTM ion microprobe facility is supported by the Carnegie Institution of Washington and NSF grants EAR9711348 and OCE97122778 to E.H.H.

References

Ackermann, L., L. Cemic, and K. Langer, Hydrogarnet substitution in pyrope: A possible location for "water" in the mantle, *Earth Planet. Sci. Lett.*, *62*, 208–214, 1983.

Aines, R. D., and G. R. Rossman, Water content of mantle garnets, *Geology*, *12*, 720–723, 1984.

Bai, Q., and D. L. Kohlstedt, Substantial hydrogen solubility in olivine and implications for water storage in the mantle, *Nature*, *357*, 672–674, 1992.

Bai, Q., and D. L. Kohlstedt, Effects of chemical environment on the solubility and incorporation mechanism for hydrogen in olivine, *Phys. Chem. Mineral.*, *19*, 460–471, 1993.

Bai, Q., Z.-C. Wang, G. Dresen, S. Mei, and D. L. Kohlstedt, Solubility and stability of hydrogen in diopside single crystals, *Eos Trans. AGU*, *75*(44), F652, Fall Meet. Suppl., 1994.

Bell, D. R., and G. R. Rossman, Water in Earth's mantle: The role of nominally anhydrous minerals, *Science*, *255*, 1391–1397, 1992a.

Bell, D. R., and G. R. Rossman, The distribution of hydroxyl in garnets from the subcontinental mantle of southern Africa, *Contrib. Mineral. Petrol.*, *111*, 161–178, 1992b.

Bell, D. R., P. D. Ihinger, and G. R. Rossman, Quantitative analysis of trace OH in garnet and pyroxenes, *Am. Mineral.*, *80*, 465–474, 1995.

Bell, D. R., G. R. Rossman, A. Maldener, D. Endisch, and F. Rauch, Hydroxide in olivine: A quantitative determination of the absolute amount and calibration of the IR spectrum, *J. Geophys. Res.*, doi:10.1029/2001JB000679, in press, 2002.

Bolfan-Casanova, N., H. Keppler, and D. Rubie, Water partitioning between nominally anhydrous minerals in the MgO-SiO_2-H_2O system up to 24 GPa: Implications for the distribution of water in the Earth's mantle, *Earth Planet. Sci. Lett.*, *182*, 209–221, 2000.

Chopra, P. M., and M. S. Paterson, The role of water in the deformation of dunite, *J. Geophys. Res.*, *89*, 7861–7876, 1984.

Deloule, E., C. France-Lanord, and F. Albarede, D/H analysis of minerals by ion probe, in "Stable Isotope Geochemistry: A Tribute to Samuel Epstein", *Geochem. Soc. Spec. Publ.*, *3*, 53–62, 1991.

Deloule, E., O. Paillat, M. Pichavant, and B. Scaillet, Ion microprobe determination of water in silicate glasses: Methods and applications, *Chem. Geol.*, *125*, 19–28, 1995.

Dixon, J. E., D. A. Clague, P. Wallace, and R. Poreda, Volatiles in alkalic basalts from the North Arch volcanic field, Hawaii: Extensive degassing of deep submarine-erupted alkalic series lavas, *J. Petrol.*, *38*, 911–939, 1997.

Dobson, P. F., H. Skogby, and G. R. Rossman, Water in boninite glass and coexisting orthopyroxene: Concentration and partitioning, *Contrib. Mineral. Petrol.*, *118*, 414–419, 1995.

Gaetani, G. A., and T. L. Grove, The influence of water on melting of mantle peridotite, *Contrib. Mineral. Petrol.*, *131*, 323–346, 1998.

Geiger, C. A., K. Langer, D. R. Bell, G. R. Rossman, and B. Winkler, The hydroxide component in synthetic pyrope, *Am. Mineral.*, *76*, 49–59, 1991.

Green, D. H., Experimental melting studies on a model upper mantle composition at high pressure under water-saturated and water-undersaturated conditions, *Earth Planet. Sci. Lett.*, *19*, 37–53, 1973.

Hauri, E., J. Wang, J. E. Dixon, P. L. King, C. Mandeville, and S. Newman, SIMS analysis of volatiles in volcanic glasses, 1, Calibration, matrix effects and comparisons with FTIR, *Chem. Geol.*, *183*, 99–114, 2002.

Hinthorne, J. R., and C. A. Andersen, Microanalysis for fluorine and hydrogen in silicates with the ion microprobe mass analyzer, *Am. Mineral.*, *60*, 143–147, 1975.

Hirose, K., and T. Kawamoto, Hydrous partial melting of lherzolite at 1 GPa: The effect of H_2O on the genesis of basaltic magmas, *Earth Planet. Sci. Lett.*, *133*, 463–473, 1995.

Hirth, G., and D. L. Kohlstedt, Water in the oceanic upper mantle: Implications for rheology, melt extraction and the evolution of the lithosphere, *Earth Planet. Sci. Lett.*, *144*, 93–108, 1996.

Ihinger, P. D., R. L. Hervig, and P. F. McMillan, Analytical methods for volatiles in glasses, in *Volatiles in Magmas*, edited by M. Carroll and J. Holloway, pp. 67–121, Mineral. Soc of Am., Washington, D.C., 1994.

Ingrin, J., S. Hercule, and T. Charton, Diffusion of hydrogen in diopside: Results of dehydration experiments, *J. Geophys. Res.*, *100*, 15,489–15,499, 1995.

Inoue, T., H. Yurimoto, and Y. Kudoh, Hydrous modified spinel, $Mg_{1.75}SiH_{0.5}O_4$: A new water reservoir in the mantle trasition region, *Geophys. Res. Lett.*, *22*, 117–120, 1995.

Inoue, T., D. J. Weidner, P. A. Northrup, and J. B. Parise, Elastic properties of hydrous ringwoodite (γ-phase) in Mg_2SiO_4, *Earth Planet. Sci. Lett.*, *160*, 107–113, 1998.

Karato, S., The role of hydrogen in the electrical conductivity of the upper mantle, *Nature*, *347*, 272–273, 1990.

Karato, S., and H. Jung, Water, partial melting and the origin of the seismic low velocity and high attenuation zone in the upper mantle, *Earth Planet. Sci. Lett.*, *157*, 193–207, 1998.

Karato, S.-I., M. Paterson, and J. D. FitzGerald, Rheology of synthetic olivine aggregates: Influence of grain size and water, *J. Geophys. Res.*, *91*, 8151–8176, 1986.

Kawamoto, T., and J. R. Holloway, Melting temperature and partial melt chemistry of H_2O-saturated mantle peridotite to 11 GPa, *Science*, *276*, 240–243, 1997.

Kohlstedt, D. L., H. Keppler, and D. C. Rubie, Solubility of water in the a, b, and c phases of (Mg,Fe)2SiO4, *Contrib. Mineral. Petrol.*, *123*, 345–357, 1996.

Kohn, S. C., Solubility of H_2O in nominally anhydrous mantle minerals using ^1H MAS NMR, *Am. Mineral.*, *81*, 1523–1526, 1996.

Kurosawa, M., H. Yurimoto, K. Matsumoto, and S. Sueno, Hydrogen analysis of mantle olivine by secondary ion mass spectrometry, in *High-Pressure Research: Application to Earth and Planetary Sciences*, edited by Y. Syono and M. H. Manghnani, pp. 283–287, Terra Sci., Tokyo, 1992.

Kurosawa, M., H. Yurimoto, and S. Sueno, Pattern in the hydrogen and trace element compositions of mantle olivine, *Phys. Chem. Miner.*, *24*, 385–395, 1997.

Kushiro, I., Effect of water on the composition of magmas formed at high pressures, *J. Petrol.*, *13*, 311–334, 1969.

Kushiro, I., Partial melting of the mantle wedge and evolution of island arc crust, *J. Geophys. Res.*, *95*, 15,929–15,939, 1972.

Libowitzky, E., and A. Beran, OH defects in forsterite, *Phys. Chem. Mineral.*, *22*, 387–392, 1995.

Libowitzky, E., and G. R. Rossman, Principles of quantitative absorbance measurements in anisotropic crystals, *Phys. Chem. Mineral.*, *23*, 319–327, 1996.

Libowitzky, E., and G. R. Rossman, An IR absorption calibration for water in minerals, *Am. Mineral.*, *82*, 1111–1115, 1997.

Lu, R., and H. Keppler, Water solubility in pyrope to 100 kbar, *Contrib. Mineral. Petrol.*, *129*, 35–42, 1997.

Mackwell, S. J., and D. L. Kohlstedt, Diffusion of hydrogen in olivine: implications for water in the mantle, *J. Geophys. Res.*, *95*, 5079–5088, 1990.

Matveev, S., H. S. C. O'Neill, C. Ballhaus, W. R. Taylor, and D. H. Green, Effect of silica activity on OH^- IR spectra of olivine: Implications for low-aSiO_2 mantle metasomatism, *J. Petrol.*, *42*, 721–729, 2001.

Meade, C., J. A. Reffner, and E. Ito, Synchrotron infrared absorbance measurements of hydrogen in $MgSiO_3$ perovskite, *Science*, *246*, 1024–1026, 1994.

Mei, S., and D. L. Kohlstedt, Influence of water on plastic deformation of olivine aggregates, 1, Diffusion creep regime, *J. Geophys. Res.*, *105*, 21,457–21,469, 2000a.

Mei, S., and D. L. Kohlstedt, Influence of water on plastic deformation of olivine aggregates, 2, Dislocation creep regime, *J. Geophys. Res.*, *105*, 21,471–21,481, 2000b.

Michael, P. J., The concentration, behavior and storage of H_2O in the suboceanic upper mantle: Implications for mantle metasomatism, *Geochim. Cosmochim. Acta*, *52*, 555–566, 1988.

Michael, P., Regionally distinctive sources of depleted MORB: Evidence from trace elements and H_2O, *Earth Planet. Sci. Lett.*, *131*, 301–320, 1995.

Miller, G. H., G. R. Rossman, and G. E. Harlow, The natural occurence of hydroxide in olivine, *Phys. Chem. Mineral.*, *14*, 461–472, 1987.

Morioka, M., Cation diffusion in olivine, 1, Cobalt and magnesium, *Geochim. Cosmochim. Acta*, *44*, 759–762, 1980.

Murakami, M., K. Hirose, H. Yurimoto, S. Nakashima, and N. Takefuji, Water in earth's lower mantle, *Science*, *295*, 1885–1887, 2002.

Mysen, B. O., and A. L. Boettcher, Melting of a hydrous upper mantle, I, Phase equilibria of a natural peridotite at high pressures and high temperatures as a function of controlled activities of water, hydrogen and carbon dioxide, *J. Petrol.*, *16*, 520–548, 1975a.

Mysen, B. O., and A. L. Boettcher, Melting of a hydrous upper mantle, I, Geochemistry of crystals and liquid formed by anatexis of mantle peridotite at high pressures and high temperatures as a function of controlled activities of water, hydrogen and carbon dioxide, *J. Petrol.*, *16*, 549–593, 1975b.

Paterson, M. S., The determination of hydroxyl by infrared absorption in quartz, silicate glasses and similar materials, *Bull. Mineral.*, *105*, 20–29, 1982.

Salters, V. J. M., J. E. Longhi, and M. Bizimis, Near mantle solidus trace element partitioning at pressures up to 3.4 GPa, *Geochem. Geophys. Geosys.*, *3*(7), 1038, doi:10.1029/2001GC000148, 2002.

Shimizu, N., and S. R. Hart, Application of the ion microprobe to geochemistry and cosmochemistry, *Annu. Rev. Earth Planet. Sci.*, *10*, 483–526, 1982.

Sisson, T. W., and G. D. Layne, H_2O in basalt and basaltic andesite glass inclusions from four subduction-related volcanoes, *Earth Planet. Sci. Lett.*, *117*, 619–635, 1993.

Skogby, H. S., OH incorporation in synthetic clinopyroxene, *Am. Mineral.*, *79*, 240–249, 1994.

Smyth, J. R., D. R. Bell, and G. R. Rossman, Incorporattion of hydroxyl in upper-mantle clinopyroxenes, *Nature*, *351*, 732–735, 1991.

Snyder, R. A., L. A. Taylor, E. A. Jerde, R. N. Clayton, T. K. Mayeda, P. Deines, G. R. Rossman, and N. V. Sobolev, Archaen mantle heterogeneity and origin of diamondiferous eclogites, Siberia: Evidence from stable isotopes and hydroxyl in garnet, *Am. Mineral.*, *80*, 799–809, 1995.

Sobolev, A. V., and M. Chaussidon, H_2O concentration in primary melts from supra-subduction zones and mid-ocean ridges: Implications for H_2O storage and recycling in the mantle, *Earth Planet. Sci. Lett.*, *137*, 45–55, 1996.

Sweeney, R. J., V. M. Prozesky, and K. A. Springhorn, Use of elastic recoil detection analysis (ERDA) microbeam technique for the quantitative determination of hydrogen in materials and hydrogen partitioning between olivine and melt at high pressures, *Geochim. Cosmochim. Acta*, *61*, 101–113, 1997.

Withers, A. C., B. J. Wood, and M. R. Carroll, The OH content of pyrope at high pressure, *Chem. Geol.*, *147*, 161–171, 1998.

Xirouchakis, D., M. M. Hirschmann, and J. A. Simpson, The effect of titanium on the silica content and on mineral-liquid partitioning of mantle-equilibrated melts, *Geochim. Cosmochim. Acta*, *65*, 2201–2217, 2001.

York, D., Least squares fitting of a straight line with correlated errors, *Earth Planet. Sci. Lett.*, *5*, 320–324, 1969.

Yurimoto, H., M. Kurosawa, and S. Sueno, Hydrogen analysis in quartz crystals and quartz glasses by secondary ion mass spectrometry, *Geochim. Cosmochim. Acta*, *53*, 751–755, 1989.